

Elliptic flow in U+U collisions at $\sqrt{s_{NN}} = 200$ GeV and in Pb+Pb collisions at $\sqrt{s_{NN}} = 2.76$ TeV: Prediction from a hybrid approach

Tetsufumi Hirano,^{1,2,*} Pasi Huovinen,^{3,†} and Yasushi Nara^{4,‡}

¹*Department of Physics, The University of Tokyo, Tokyo 113-0033, Japan*

²*Nuclear Science Division, Lawrence Berkeley National Laboratory, Berkeley, CA 94720, USA*

³*Institut für Theoretische Physik, Johann Wolfgang Goethe-Universität, 60438 Frankfurt am Main, Germany*

⁴*Akita International University, Yuwa, Akita-city 010-1292, Japan*

(Dated: November 19, 2018)

We predict the elliptic flow parameter v_2 in U+U collisions at $\sqrt{s_{NN}} = 200$ GeV and in Pb+Pb collisions at $\sqrt{s_{NN}} = 2.76$ TeV using a hybrid model in which the evolution of the quark gluon plasma is described by ideal hydrodynamics with a state-of-the-art lattice QCD equation of state, and the subsequent hadronic stage by a hadron cascade model.

PACS numbers: 25.75.-q, 25.75.Nq, 12.38.Mh, 12.38.Qk

One of the major discoveries at Relativistic Heavy Ion Collider (RHIC) in Brookhaven National Laboratory (BNL) was that for the first time in relativistic heavy ion collisions, the elliptic flow appeared to be as large as an ideal hydrodynamic prediction [1]. Since viscosity and any other dissipative effects vanish in ideal hydrodynamics, and tiny viscosity requires a strong coupling of constituents (quarks and gluons in our case), this discovery established the new paradigm of strongly coupled quark gluon plasma [2, 3].

In noncentral collisions, rescatterings of the created particles convert the initial spatial anisotropy of the reaction zone to anisotropic particle distribution [4]. Ideal hydrodynamics predicts that the ratio of these anisotropies is $v_2/\varepsilon \sim 0.2$ almost independent of centrality at the RHIC energies [5]. Here v_2 is the second Fourier coefficient of the azimuthal distribution of final particles, and ε is the initial eccentricity of the produced matter. On the other hand, in the dilute regime kinetic theory predicts v_2 to be proportional to the particle multiplicity per unit rapidity, dN/dy [6, 7]. Thus, the response of the system, v_2/ε , provides information about the transport properties of the QGP. Experimentally v_2/ε is seen to increase with increasing transverse density $(1/S)dN/dy$ [8, 9], where S is the transverse area of the collision zone, until it reaches the so-called hydrodynamic limit, $v_2/\varepsilon \sim 0.2$, in central Au+Au collisions at RHIC. With the agreement of the hydrodynamical prediction of the particle mass dependence of $v_2(p_T)$ [10] with the data [11, 12], this is considered as evidence for the discovery of the perfect-fluid nature of the QGP [1].

After observing the increase of v_2/ε with increasing transverse density, it is natural to ask what happens if the transverse density increases beyond that achieved at RHIC [13]. Will it saturate to the value observed at RHIC, as expected if the system behaves like a perfect

fluid, or will it keep increasing? One suggested way to extend the transverse density is to perform uranium-uranium collisions [13]. Since uranium nuclei are deformed and larger than gold nuclei, one can expect large transverse density with finite eccentricity in the body-body collisions at vanishing impact parameter¹. Some Monte Carlo studies show that, even though one cannot control the orientation of colliding nuclei, events with high multiplicity though finite eccentricity can be selected in the usual triggering process [13, 15–18]. Another way to extend the transverse energy is to increase the collision energy to generate more particles in collisions. This is going to happen very soon in the Large Hadron Collider (LHC) heavy ion program. In this Rapid Communication we predict elliptic flow parameters both in U+U collisions at RHIC and Pb+Pb collisions at LHC using a hybrid model based on ideal hydrodynamics and hadron cascade.

We describe space-time evolution of the QGP by ideal hydrodynamics [19] with the recent lattice QCD equation of state [20]. After expansion and cooling, the system turns into hadronic matter. We switch from hydrodynamics to a kinetic approach at a switching temperature T_{sw} and employ a hadronic cascade model, JAM [21], to describe the subsequent space-time evolution of hadronic matter.

Our EoS, *s95p-v1.1*, is a slightly modified version of the *s95p-v1* EoS presented in [20]. It interpolates between hadron resonance gas at low temperatures, and recent lattice QCD results by the hotQCD collaboration [22, 23] at high temperatures in the same way as *s95p-v1*, but the hadron resonance gas part contains the same hadrons and resonances as the JAM hadron cascade [21]. The details of the interpolating procedure are explained in [20] and the parametrization and EoS tables are available at [24].

For initial conditions, we employ two Monte-Carlo approaches to simulate collisions of two energetic

* hirano@phys.s.u-tokyo.ac.jp

† huovinen@th.physik.uni-frankfurt.de

‡ nara@aiu.ac.jp

¹ The idea of collisions of deformed nuclei is not new and one can find literature on this subject. See, e.g., Refs. [5, 14].

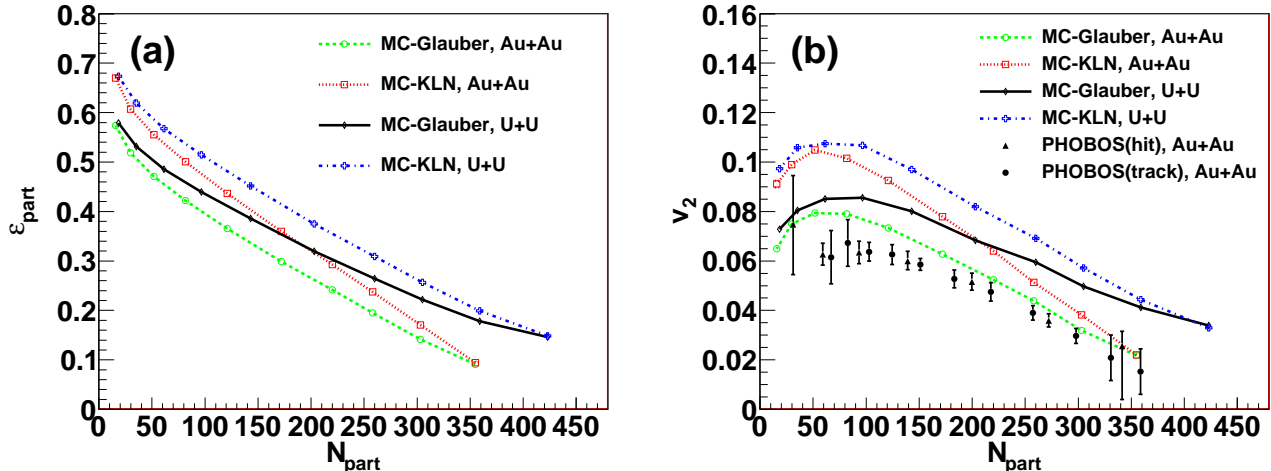


FIG. 1. (Color online) (a) Initial state eccentricity $\varepsilon_{\text{part}}$ and (b) v_2 as a function of N_{part} in Au+Au and U+U collisions at $\sqrt{s_{NN}} = 200$ GeV. Experimental data of v_2 in Au+Au collisions are obtained by PHOBOS Collaboration [34].

nuclei: Monte-Carlo Glauber (MC-Glauber) model [25] and Monte-Carlo Kharzeev-Levin-Nardi (MC-KLN) model [26]. In the MC-Glauber model, one calculates the number of participants N_{part} and the number of binary collisions N_{coll} for a given nuclear density distribution. We model the initial entropy distribution in hydrodynamic simulations as a linear combination of the number distribution of participants $\rho_{\text{part}} = \frac{dN_{\text{part}}}{d^2\mathbf{x}_{\perp}}$ and that of binary collisions $\rho_{\text{coll}} = \frac{dN_{\text{coll}}}{d^2\mathbf{x}_{\perp}}$ in the transverse plane:

$$\frac{dS}{d^2\mathbf{x}_{\perp}} \propto \frac{1-\alpha}{2}\rho_{\text{part}}(\mathbf{x}_{\perp}) + \alpha\rho_{\text{coll}}(\mathbf{x}_{\perp}). \quad (1)$$

We generate the number distributions in an event-by-event basis, align them to match the main and sub axes of the ellipsoids, and average over many events for a given centrality bin to obtain a smooth distribution [27]. The eccentricity of the initial profile is then evaluated with respect to participant plane, $\varepsilon_{\text{part}}$ [28]. We do the centrality cuts according to the N_{part} distribution from the MC-Glauber model instead of using the optical Glauber limit as was done in Ref. [27]. The free parameters of the model, the mixing parameter $\alpha = 0.18$ and the proportionality constant in Eq. (1), are chosen to reproduce transverse momentum spectra for pions, kaons, and protons from central (0-5%) to peripheral (70-80%) events in Au+Au collisions at $\sqrt{s_{NN}} = 200$ GeV obtained by the PHENIX Collaboration [29]. We also choose the switching temperature as $T_{\text{sw}} = 155$ MeV to describe the relative yields for pions, kaons, and protons in these data.

MC-KLN model is a Monte Carlo version of the factorized Kharzeev-Levin-Nardi (fKLN) model [30]. In the MC-KLN model, gluon production is obtained by numerical integration of the k_t -factorized formula [31] at each transverse grid. The fluctuation of gluon distribution due to the position of hard sources (nucleons) in the transverse plane is taken into account in MC-KLN. Using

the thickness function T_A , we parametrize the saturation scale for a nucleus A as

$$Q_{s,A}^2(x; \mathbf{x}_{\perp}) = 2 \text{ GeV}^2 \frac{T_A(\mathbf{x}_{\perp})}{1.53 \text{ fm}^{-2}} \left(\frac{0.01}{x}\right)^{\lambda} \quad (2)$$

and similarly for a nucleus B. We choose $\lambda = 0.28$ and a proportionality constant in the unintegrated gluon distribution in the k_t -factorized formula to reproduce centrality dependence of p_T spectra for pions, kaons, and protons as above.

Using the same parameter set as above, we calculate initial entropy distribution in U+U collisions by changing the nuclear density from gold to uranium. To take account of the prolate deformation of uranium nuclei, we parametrize the radius parameter in the Woods-Saxon distribution as

$$R(\theta, \phi) = R_0 (1 + \beta_2 Y_{20}(\theta, \phi) + \beta_4 Y_{40}(\theta, \phi)), \quad (3)$$

where Y_{lm} is the spherical harmonic function, $R_0 = 6.86$ fm, $\beta_2 = 0.28$ and $\beta_4 = 0.093$ [32]. Note that to account of the finite size of nucleons in the Monte Carlo approach, we have adjusted R_0 above and the diffuseness parameter $\delta r = 0.44$ to retain the nuclear density as in the original Woods-Saxon distribution [27]. We also take into account that colliding uranium nuclei are randomly oriented in each event.

Figure 1 (a) shows initial eccentricity with respect to participant plane in Au+Au and U+U collisions at $\sqrt{s_{NN}} = 200$ GeV as a function of the number of participants. At each of the ten centrality bins the average eccentricity and the average number of participants $\langle N_{\text{part}} \rangle$ were calculated using both the MC-Glauber and the MC-KLN models. Since the eccentricity is measured in the participant plane, it is finite even in the very central (0-5%) Au+Au collisions. As previously known, the MC-KLN model leads to ~ 20 -30% larger eccentricity than

the MC-Glauber model except in the most central events [30, 33]. In most central 5% of U+U collisions eccentricity reaches 0.146 in the MC-Glauber model and 0.148 in the MC-KLN model. The eccentricity is larger in U+U than in Au+Au collisions. Due to the deformed shape of uranium nucleus, this holds not only at fixed number of participants, but also at fixed centrality. The difference, however, decreases with decreasing centrality, and there is almost no difference in the very peripheral events (70-80%).

In Fig. 1 (b), v_2 in Au+Au collisions is compared with the v_2 in U+U collisions. Since the rule of thumb is that larger eccentricity leads to larger momentum anisotropy and v_2 , the systematics of $v_2(N_{\text{part}})$ is similar to that of $\varepsilon_{\text{part}}(N_{\text{part}})$: v_2 is larger in U+U collisions than in Au+Au collisions, and MC-KLN initialization leads to larger v_2 than MC-Glauber initialization. As well, v_2 first increases with decreasing N_{part} , which reflects increasing initial eccentricity, but once N_{part} falls below ~ 50 , v_2 begins to decrease. This is due to the short lifetime of the system which does not allow the flow to fully build up, and to the large fraction of the lifetime spent in the hadronic phase where dissipative effects are large.

Results from the MC-Glauber initialization almost reproduce the PHOBOS data [34] in Au+Au collisions. This indicates that there is little room for QGP viscosity in the model calculations. On the other hand, apparent discrepancy between the results from the MC-KLN initialization and the PHOBOS data means that viscous corrections during the plasma phase are required.

Within the color glass condensate picture, the collision energy dependence is taken into account through the saturation scale, Q_s . This allows us to simulate the Pb+Pb collisions at $\sqrt{s_{NN}} = 2.76$ TeV by using the MC-KLN model, adjusting the collision energy parameter and the nuclear density parametrization, and keeping all the other parameters unchanged. This is a consistent way to study the differences between collisions at $\sqrt{s_{NN}} = 62.4$ GeV and 2.76 TeV energies, but it may be too naive, since the MC-KLN model does not take into account running coupling corrections to the evolution equation [35]. At RHIC energies these effects are known to have only a small effect, but at LHC they lead to a clearly lower multiplicity [35, 36]. On the other hand, these effects hardly affect the eccentricity [36], which allows us to study the effects of the uncertainty in the final particle multiplicity simply by adjusting the overall factor in the unintegrated gluon distribution function. Our default approach is to use the MC-KLN model with the same factor than in the RHIC calculations. In 5% most central Pb+Pb collisions this leads to multiplicity $dN_{\text{ch}}/d\eta \sim 1600$ at midrapidity ($|\eta| < 1$). We also reduce the factor to obtain multiplicities $dN_{\text{ch}}/d\eta \sim 1400$ (set 1), as predicted in Ref. [35], and ~ 1200 (set 2)².

Our result for the initial state eccentricity as function of the number of participants in Au+Au collisions at $\sqrt{s_{NN}} = 200$ GeV, and in Pb+Pb collisions at $\sqrt{s_{NN}} = 2.76$ TeV is shown in Fig. 2 (a). As mentioned, the uncertainty in the multiplicity in collisions at $\sqrt{s_{NN}} = 2.76$ TeV does not affect the eccentricity and we show the result obtained using our default setting. For a fixed N_{part} , eccentricity at LHC is apparently larger than that at RHIC. However, this is due solely to the larger size of colliding nuclei. If one compares the eccentricity at a fixed centrality (see each point in the figure), eccentricities are essentially the same.

In Fig. 2 (b), v_2 in Pb+Pb collisions at $\sqrt{s_{NN}} = 2.76$ TeV is shown as a function of the number of participants for three different multiplicities in central collisions. The larger the multiplicity, the larger the v_2 , but even at the lowest setting of multiplicity, v_2 is clearly larger than in the Au+Au collisions at $\sqrt{s_{NN}} = 200$ GeV.

This behavior is clearly visible in Fig. 3 where we plot $v_2/\varepsilon_{\text{part}}$ as a function of the transverse charged particle density $(1/S)dN_{\text{ch}}/d\eta$ at midrapidity ($|\eta| < 1$) for various collision systems and energies. First, as expected, the system in U+U collisions at $\sqrt{s_{NN}} = 200$ GeV is denser than in Au+Au collisions at the same energy. At initial time $\tau_0 = 0.6$ fm/c, the maximum temperature (energy density) in the most central 5% of U+U collisions is $T_0 = 367$ MeV ($e_0 = 33.4$ GeV/fm³) and $T_0 = 361$ MeV ($e_0 = 31.4$ GeV/fm³) in the Au+Au collisions of the same centrality. This corresponds to charged particle transverse densities of 25.4 and 24.1, respectively, which means that the transverse density in U+U collisions is indeed larger, but only by $\sim 6\%$ ³. In spite of the differences in the colliding systems, results for various centralities in U+U collisions almost trace the ones in Au+Au collisions, which would suggest existence of scaling behavior in $v_2/\varepsilon_{\text{part}}$ versus $(1/S)dN_{\text{ch}}/d\eta$.

However, the behavior of $v_2/\varepsilon_{\text{part}}$ in Pb+Pb collisions at $\sqrt{s_{NN}} = 2.76$ TeV is very different. In these collisions the system is much denser than in the collisions at RHIC energies. The maximum temperature at the initial time $\tau_0 = 0.6$ fm/c is $T_0 = 474, 456, 436$ MeV ($e_0 = 96.2, 81.7, 67.8$ GeV/fm³) for $dN_{\text{ch}}/d\eta \sim 1600, 1400, 1200$ in 5% most central collisions, respectively, which corresponds to roughly 2–2.5 times larger transverse density than in most central Au+Au collisions at $\sqrt{s_{NN}} = 200$ GeV. As can be seen, $v_2/\varepsilon_{\text{part}}$ no longer follows the scaling curve seen at the top RHIC energy, but it reaches ~ 0.26 – 0.3 in central collisions. This value is ~ 20 – 35% larger than the value at RHIC, which is often considered a hydrodynamical upper limit in the literature [37].

The reason for this breaking of the scaling is not in the cascade treatment of the hadronic phase. If any-

² η is not the shear viscous coefficient but the pseudorapidity.

³ With sufficient statistics, one may make more severe centrality cut (e.g., 0-3%) to obtain larger transverse particle density. Multiplicity fluctuation in the centrality cut, which we do not take into account, could also enhance the transverse particle density.

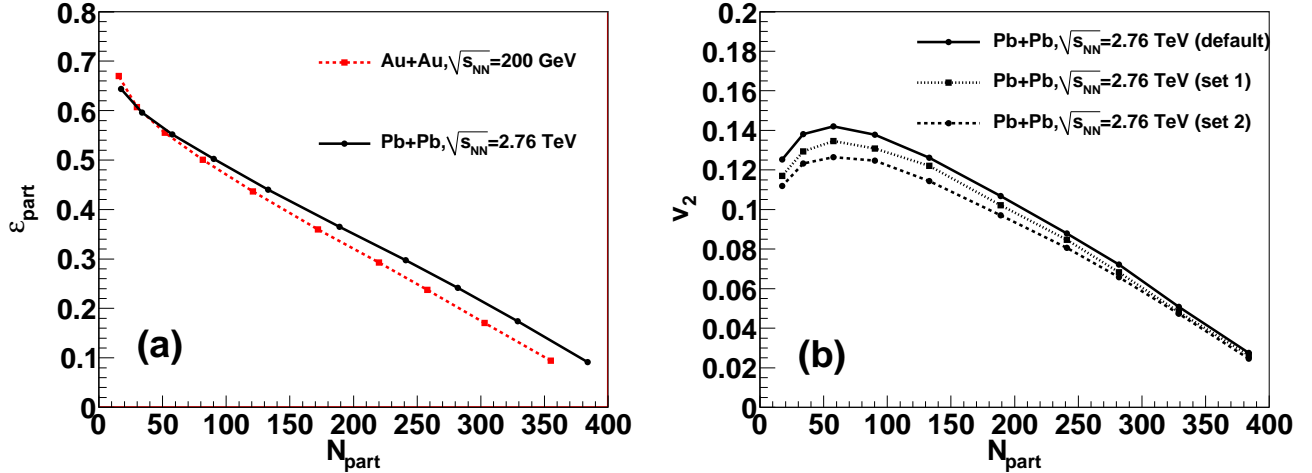


FIG. 2. (Color online) (a) $\varepsilon_{\text{part}}$ as a function of N_{part} in Au+Au collisions at $\sqrt{s_{NN}} = 200$ GeV (dashed) and in Pb+Pb collisions at $\sqrt{s_{NN}} = 2.76$ TeV (solid). (b) v_2 as function of number of participants N_{part} in Pb+Pb collisions at $\sqrt{s_{NN}} = 2.76$ TeV for three different multiplicities in 0-5% centrality: $dN_{\text{ch}}/d\eta \sim 1600$ (solid), 1400 (dotted) and 1200 (dashed). Each point from right to left corresponds to 0-5, 5-10, 10-15, 15-20, 20-30, 30-40, 40-50, 50-60, 60-70, and 70-80% centrality, respectively.

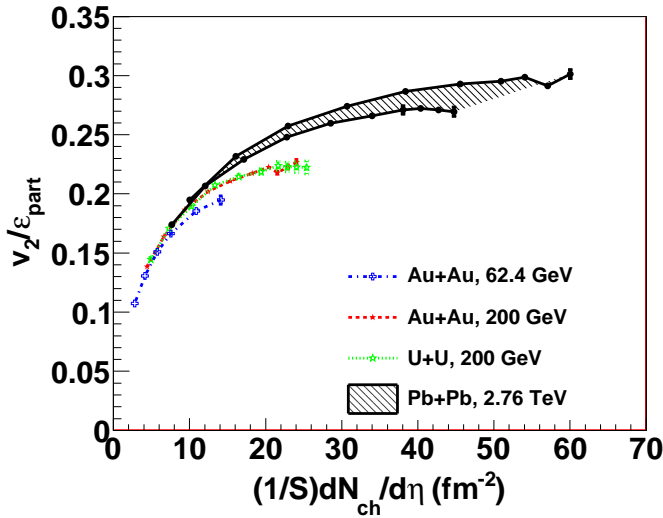


FIG. 3. $v_2/\varepsilon_{\text{part}}$ as a function of transverse density in Au+Au collisions at $\sqrt{s_{NN}} = 62.4$ (dash-dotted) and 200 GeV (dashed), in U+U collisions at $\sqrt{s_{NN}} = 200$ GeV (dotted), and in Pb+Pb collisions at $\sqrt{s_{NN}} = 2.76$ TeV (band). The band depicting the Pb+Pb collisions spans the results obtained using the multiplicities $1200 < dN_{\text{ch}}/d\eta < 1600$ in 5% most central central collisions.

thing, dissipation should reduce v_2 , so hadron cascade cannot be responsible for the large value of $v_2/\varepsilon_{\text{part}}$ seen here. We have also checked that at LHC, the major part of v_2 is generated during the hydrodynamical stage, and the effects of hadronic cascade are less important than at RHIC. The ratio of v_2 generated during the hydrodynamical evolution to the final v_2 , $v_{2,\text{fluid}}/v_2$, in collisions at RHIC and LHC is shown in Fig. 4. As can be seen, the contribution of hadronic cascade to the total v_2 with de-

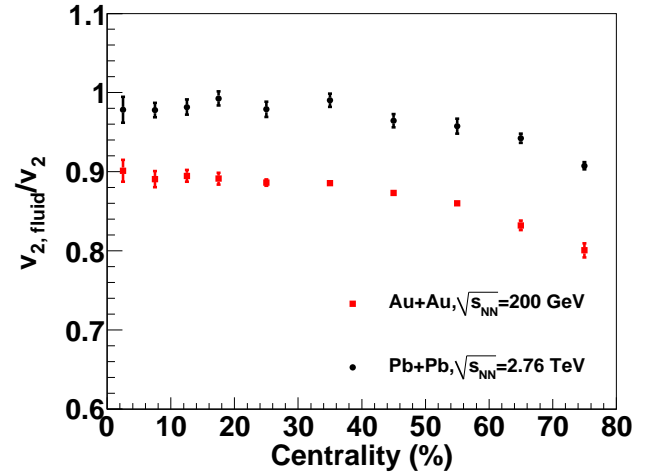


FIG. 4. The ratio of v_2 generated during the hydrodynamical evolution to the final v_2 , $v_{2,\text{fluid}}/v_2$, in Au+Au and Pb+Pb collisions at $\sqrt{s_{NN}} = 200$ GeV and 2.76 TeV, respectively.

fault setting at LHC is less than 5% at most centralities. On the other hand, the contribution reaches 10-20% of the total v_2 in Au+Au collisions at the top RHIC energy.

To further study the collision energy dependence of $v_2/\varepsilon_{\text{part}}$, we do the calculation using the lower RHIC energy $\sqrt{s_{NN}} = 62.4$ GeV. As seen in Fig. 3, the ratio in central collisions (0-30%) deviates from the scaling curve seen at $\sqrt{s_{NN}} = 200$ GeV, but the amount of the deviation might be too small to be experimentally observable. The collision energy independence of $v_2/\varepsilon_{\text{part}}$ is seen in $(1/S)dN_{\text{ch}}/d\eta \lesssim 10$ (fm^{-2}) which corresponds to $dN_{\text{ch}}/d\eta \lesssim 50$ where hadronic cascading plays a major

role in the whole evolution. Note that the collision energy dependence of $v_2/\varepsilon_{\text{part}}$ is consistent with the early calculations where v_2 continuously increases with total pion multiplicity dN_π/dy at midrapidity up to 3000 at a fixed impact parameter ($b = 7$ fm) [5]. See also Ref. [38] for a previous calculation in which the bag model equation of state and a higher switching temperature $T_{\text{sw}} = 169$ MeV were used.

Recently, a prediction of elliptic flow as a function of transverse charged particle density up to the LHC energies was made using viscous hydrodynamics in Ref. [39]. To avoid the uncertainties associated with the freeze-out process, v_2 was evaluated in that paper by calculating the momentum anisotropy

$$e_p = \frac{\int dx dy (T^{xx} - T^{yy})}{\int dx dy (T^{xx} + T^{yy})} \quad (4)$$

and relying on an empirical formula $v_2 \approx e_p/2$ [40]. We have checked the validity of this formula in our calculations, and found that in the collisions at the LHC energy, the ratio is rather $v_2/e_p \approx 2/3$, not $1/2$. This discrepancy is not surprising. First, it is known that the ratio strongly depends on the freeze-out temperature [41]. The momentum anisotropy depicts the anisotropy of the collective motion, whereas v_2 reflects the anisotropy of the momenta of individual particles, which includes thermal motion, the effects due to resonance decays [42] and to the shape of the source [43]. Second, the formula was found to hold in ideal fluid calculations. How dissipation affects it cannot be calculated, but has to be observed on case by case basis.

To summarize, we predicted elliptic flow parameter v_2

in U+U collisions at $\sqrt{s_{NN}} = 200$ GeV and in Pb+Pb collisions at $\sqrt{s_{NN}} = 2.76$ TeV using a hybrid approach which combines ideal hydrodynamic description of the QGP fluid and kinetic description of the hadronic gas. Due to deformation of uranium, eccentricity is larger in U+U collisions than in Au+Au collisions. We found the maximum transverse particle density is $\sim 6\%$ larger in 0-5% central U+U collisions. $v_2/\varepsilon_{\text{part}}$ in U+U collisions follows the results in Au+Au collisions, which suggests a scaling behavior between $v_2/\varepsilon_{\text{part}}$ and $(1/S)dN_{\text{ch}}/d\eta$. However, at the LHC energy, $v_2/\varepsilon_{\text{part}}$ does *not* follow the same scaling curve and reaches the maximum value of ~ 0.26 – 0.30 depending on the final particle multiplicity. This is clearly larger than the corresponding maximum value at the top RHIC energy, $v_2/\varepsilon_{\text{part}} \sim 0.22$, and the so-called hydrodynamic limit for v_2/ε is not the same at RHIC and LHC energies.

ACKNOWLEDGMENTS

The work of T.H. (Y.N.) was partly supported by Grant-in-Aid for Scientific Research No. 22740151 (No. 20540276). T.H. is also supported under Excellent Young Researchers Oversea Visit Program (No. 21-3383) by Japan Society for the Promotion of Science. P.H.'s work is supported by the ExtreMe Matter Institute (EMMI). We acknowledge fruitful discussion with A. Dumitru. T.H. thanks members in the nuclear theory group at Lawrence Berkeley National Laboratory for a kind hospitality during his sabbatical stay and M. Gyulassy for his suggestion to calculate v_2 at the LHC energies.

-
- [1] http://www.bnl.gov/bnlweb/pubaf/pr/PR_display.asp?prID=05-38.
[2] M. Gyulassy, arXiv:nucl-th/0403032.
[3] T. D. Lee, Nucl. Phys. A **750**, 1 (2005); M. Gyulassy and L. McLerran, Nucl. Phys. A **750**, 30 (2005); E. V. Shuryak, Nucl. Phys. A **750**, 64 (2005).
[4] J. Y. Ollitrault, Phys. Rev. D **46**, 229 (1992).
[5] P. F. Kolb, J. Sollfrank, and U. W. Heinz, Phys. Rev. **C62**, 054909 (2000).
[6] H. Heiselberg and A. -M. Levy, Phys. Rev. **C59**, 2716-2727 (1999).
[7] P. F. Kolb, P. Huovinen, U. W. Heinz, and H. Heiselberg, Phys. Lett. B **500**, 232 (2001).
[8] C. Adler *et al.* [STAR Collaboration], Phys. Rev. C **66**, 034904 (2002).
[9] C. Alt *et al.* [NA49 Collaboration], Phys. Rev. C **68**, 034903 (2003).
[10] P. Huovinen, P. F. Kolb, U. W. Heinz, P. V. Ruuskanen, and S. A. Voloshin, Phys. Lett. B **503**, 58 (2001).
[11] J. Adams *et al.* [STAR Collaboration], Phys. Rev. Lett. **92**, 052302 (2004).
[12] S. S. Adler *et al.* [PHENIX Collaboration], Phys. Rev. Lett. **91**, 182301 (2003).
[13] U. W. Heinz and A. Kuhlman, Phys. Rev. Lett. **94**, 132301 (2005).
[14] C. Nonaka, E. Honda, and S. Muroya, Eur. Phys. J. C **17**, 663 (2000).
[15] A. J. Kuhlman and U. W. Heinz, Phys. Rev. C **72**, 037901 (2005).
[16] C. Nepali, G. Fai, and D. Keane, Phys. Rev. C **73**, 034911 (2006).
[17] C. Nepali, G. I. Fai, and D. Keane, Phys. Rev. C **76**, 051902 (2007) [Erratum-ibid. C **76**, 069903 (2007)].
[18] H. Masui, B. Mohanty, and N. Xu, Phys. Lett. B **679**, 440 (2009).
[19] T. Hirano, Phys. Rev. C **65**, 011901 (2002).
[20] P. Huovinen and P. Petreczky, Nucl. Phys. A **837**, 26 (2010).
[21] Y. Nara, N. Otuka, A. Ohnishi, K. Niita, and S. Chiba, Phys. Rev. C **61**, 024901 (2000).
[22] M. Cheng *et al.*, Phys. Rev. D **77**, 014511 (2008).
[23] A. Bazavov *et al.*, Phys. Rev. D **80**, 014504 (2009).
[24] https://wiki.bnl.gov/hhic/index.php/Lattice_calculatons_of_ and https://wiki.bnl.gov/TECHQM/index.php/QCD_Equation_of_S
[25] M. L. Miller, K. Reygers, S. J. Sanders, and P. Steinberg, Ann. Rev. Nucl. Part. Sci. **57**, 205 (2007).

- [26] H. J. Drescher and Y. Nara, Phys. Rev. C **75**, 034905 (2007); **76**, 041903(R) (2007).
- [27] T. Hirano and Y. Nara, Phys. Rev. C **79**, 064904 (2009).
- [28] B. Alver *et al.*, Phys. Rev. C **77**, 014906 (2008).
- [29] S. S. Adler *et al.* [PHENIX Collaboration], Phys. Rev. C **69**, 034909 (2004).
- [30] A. Adil, H. J. Drescher, A. Dumitru, A. Hayashigaki, and Y. Nara, Phys. Rev. C **74**, 044905 (2006).
- [31] D. Kharzeev and M. Nardi, Phys. Lett. **B507**, 121 (2001); D. Kharzeev and E. Levin, *ibid.* **B523**, 79 (2001); D. Kharzeev, E. Levin, and M. Nardi, Phys. Rev. C **71**, 054903 (2005); Nucl. Phys. **A730**, 448 (2004).
- [32] P. Filip, R. Lednicky, H. Masui, and N. Xu, Phys. Rev. C **80**, 054903 (2009).
- [33] T. Hirano, U. W. Heinz, D. Kharzeev, R. Lacey, and Y. Nara, Phys. Lett. B **636**, 299 (2006).
- [34] B. B. Back *et al.* [PHOBOS Collaboration], Phys. Rev. C **72**, 051901 (2005).
- [35] J. L. Albacete, Phys. Rev. Lett. **99**, 262301 (2007).
- [36] A. Dumitru, private communication; http://physics.baruch.cuny.edu/node/people/adumitru/res_cg
- [37] S. A. Voloshin, A. M. Poskanzer and R. Snellings, arXiv:0809.2949 [nucl-ex].
- [38] T. Hirano, U. W. Heinz, D. Kharzeev, R. Lacey, and Y. Nara, J. Phys. G **34**, S879 (2007).
- [39] M. Luzum and P. Romatschke, Phys. Rev. Lett. **103**, 262302 (2009).
- [40] P. F. Kolb, J. Sollfrank, and U. W. Heinz, Phys. Lett. B **459**, 667 (1999).
- [41] P. Huovinen, arXiv:nucl-th/0305064.
- [42] T. Hirano, Phys. Rev. Lett. **86**, 2754 (2001).
- [43] P. Huovinen, P. F. Kolb, and U. W. Heinz, Nucl. Phys. A **698**, 475 (2002).